Letter Vol. 43, No. 4 / 15 February 2018 / Optics Letters 743

Arbitrary shaping of biphoton correlations using near-field frequency-to-time mapping

Hsuan-Hao Lu,[1,2,†] Ogaga D. Odele,[1,2,†] Daniel E. Leaird,[1,2] and Andrew M. Weiner[1,2,3,*]

[1]School of Electrical and Computer Engineering, Purdue University, West Lafayette, Indiana 47906, USA
[2]Purdue Quantum Center, Purdue University, West Lafayette, Indiana 47906, USA
[3]Birck Nanotechnology Center, Purdue University, West Lafayette, Indiana 47906, USA
*Corresponding author: amw@purdue.edu

Received 7 November 2017; revised 4 January 2018; accepted 8 January 2018; posted 9 January 2018 (Doc. ID 312524); published 7 February 2018

Frequency-to-time mapping (FTM) is a technique used to mirror the spectral shape of an optical waveform in the time domain. The regular approach, based on the far-field condition, requires large amounts of dispersion for successful mapping. However, when the far-field condition is insurmountable for achieving a desired temporal profile, another technique, termed near-field FTM, can be employed to assist with the mapping. For the first time, we demonstrate a shaper-assisted near-field FTM using entangled photon pairs. By pre-modifying the two-photon spectral amplitude and phase before propagating the photon pairs through dispersion, we can achieve arbitrary temporal correlations in the near-field region.

OCIS codes: (270.0270) Quantum optics; (190.4410) Nonlinear optics, parametric processes; (260.2030) Dispersion; (320.5540) Pulse shaping.

https://doi.org/10.1364/OL.43.000743

At the quantum level, light can play an important role in advancing technologies for secure communication, solving computationally hard problems and improving measurement sensitivity beyond the classical limit [1]. In this regard, there has been an increased interest in developing techniques for controlling the different attributes of quantum states of light. The spectral-temporal wave function is a property of single and entangled photons that has been studied extensively in recent years; manipulation of this probability amplitude using dispersion [2–4], Fourier-transform pulse shaping [5,6], electro-optic modulation [7–9], and nonlinear mixing [10,11] have been demonstrated, and are even being tied to specific applications in quantum information processing [12–14].

Using dispersion, a well-known technique for manipulating the temporal correlations of entangled photons is frequency-to-time mapping (FTM), whereby a considerable amount of dispersion allows the temporal correlation to take on the shape of the biphoton spectrum [2,15]. For proper mapping of the spectrum into the temporal domain, the temporal *far-field* condition typically must be met: the second-order spectral phase constant should be much larger than the square of the Fourier-limited temporal width of the biphoton wave packet [2]. But what if, for a given spectral shape and desired temporal duration, the far-field limit is beyond reach?

In this Letter, we adopt a technique from classical photonics, termed *near-field* FTM [16], to demonstrate arbitrary shaping of the temporal correlations of broadband biphotons. Here, successful FTM is achieved through spectral amplitude and phase preadjustment along with smaller amounts of dispersion (compared with the far-field approach). Moreover, unlike far-field FTM, which leads to spreading of the correlations over a large temporal window, typically on the ns scale, the near-field technique can be used to address a narrower temporal range (a few ps) as it does not require substantial dispersion. Our work is an addition to the recent efforts in developing various means to tailor the temporal correlations of biphotons.

Consider an entangled photon pair generated from spontaneous parametric downconversion (SPDC) of a monochromatic pump. The second-order correlation function of the SPDC photon pair is given by $G^{(2)}(\tau) = |\psi(\tau)|^2$, where $\psi(\tau)$ is referred to as the effective biphoton wave packet [17]. Prior to any manipulation, the two-photon temporal wave packet $\psi_{\text{in}}(\tau)$ is related to the two-photon spectral amplitude $\phi_{\text{in}}(\Omega)$ through the Fourier transformation

$$\psi_{\text{in}}(\tau) = \int \mathrm{d}\Omega \phi_{\text{in}}(\Omega) e^{-i\Omega\tau}. \tag{1}$$

Propagation of the biphoton in a dispersive medium with a net quadratic spectral phase constant, A_2 [ps]^2 modifies the wave packet as follows [2]:

$$\psi_{\text{out}}(\tau) \propto \int \mathrm{d}\Omega \phi_{\text{in}}(\Omega) e^{iA_2\Omega^2/2} e^{-i\Omega\tau}, \tag{2}$$

which we can also formulate in the time domain to yield a Fresnel integral:

$$\psi_{\text{out}}(\tau) \propto e^{-i\tau^2/2A_2} \int \mathrm{d}\tau' \psi_{\text{in}}(\tau') e^{-i\tau'^2/2A_2} e^{i\tau\tau'/A_2}. \tag{3}$$

The expression of the biphoton wave packet [Eq. (3)] bears a resemblance to the complex envelope of a classical pulse propagating

through dispersion; it is on this account that we adopt the mathematical procedure in [16] for the following discussion.

If the net dispersion parameter is much larger than the square of the temporal width of the biphoton wave packet (far-field condition), the first complex exponential term under the integral in Eq. (3) can be dropped as an approximation. Consequently, it would be possible to write the resulting wave function as

$$\psi_{\text{out}}(\tau) \propto \int \mathrm{d}\tau' \psi_{\text{in}}(\tau') e^{i\tau\tau'/A_2}, \tag{4}$$

which results in $G^{(2)}_{\text{out}}(\tau) = |\phi_{\text{in}}(\Omega = \tau'/A_2)|^2$, meaning that the temporal correlation is now essentially a scaled-replica of the biphoton spectrum. Demonstrations of far-field FTM have already been shown using different biphoton sources. In [2], the authors show far-field mapping of continuous broadband spectra from type-I and type-II SPDC, while in [15] strong dispersion was used to map a biphoton comb structure from a microring resonator into temporal correlations. In addition, we show far-field FTM after spectral-amplitude shaping of SPDC biphotons. Using a pulse shaper, we program three rectangular filters with bandwidths of 50, 100, and 150 GHz, on both signal and idler photons, as can be seen in Fig. 1(a). After propagating them through a chirped fiber Bragg grating with $A_2 = 5200$ ps^2, which easily meets the far-field condition, the temporal correlation now resembles the biphoton spectrum, as shown in Fig. 1(b).

On the other hand, if A_2 is not large enough to meet the far-field condition (i.e., operation is in the near-field regime), we can still obtain the expression in Eq. (4); this time, we eliminate the first complex exponential term under the integral in Eq. (3) by replacing the input wave packet with a modified version,

$$\psi_{\text{nf}}(\tau') = \psi_{\text{in}}(\tau') \times e^{i\tau'^2/2A_2}. \tag{5}$$

Therefore, irrespective of the amount of dispersion available, we are able to map a target shape to the temporal domain by preadjusting the biphoton wave packet before propagating it through dispersion. Indeed, the expression in Eq. (5) points to the utilization of quadratic temporal phase (a time lens) [18,19] for preadjustment. However, in our experiments, we realize the functionality of the time lens by applying the frequency-domain equivalent of the expression in Eq. (5) using a programmable pulse shaper; this Fourier approach is termed *virtual* time lensing [16]. Hence, our near-field shaping procedure is as follows: **(Step 1)** compute $\psi_{\text{nf}}(\tau') = \psi_{\text{in}}(\tau') \times \exp(i\tau'^2/2A_2)$; **(Step 2)** Fourier transform $\psi_{\text{nf}}(\tau')$ to its frequency-domain equivalent $\phi_{\text{nf}}(\Omega)$; **(Step 3)** apply the near-field frequency-domain mask to the biphoton using a pulse shaper; **(Step 4)** propagate the biphoton through the dispersive medium with the net dispersion constant A_2.

Our experimental setup is shown in Fig. 2(a). We couple a continuous-wave pump laser at ~774 nm into a 67-mm-long periodically poled lithium niobate (PPLN) waveguide that is temperature controlled at ~140°C for quasi-phase matching under the type-0 configuration. Frequency-degenerate broadband entangled photons centered around 1548 nm are generated through the SPDC process, and an internal efficiency of 10^{-5} per coupled pump photon is measured. The residual pump is removed with a series of colored filters, and the generated biphotons are fiber-coupled into a pulse shaper [20] (Finisar WaveShaper 1000S) capable of independent amplitude and phase control at 10 GHz resolution over the band from 191.250 to 196.275 THz.

Figure 2(b) provides the biphoton spectrum obtained directly after the collimator by an optical spectrum analyzer (OSA; Yokogawa), before passing through the 2.5 THz passbands set by the pulse shaper (dashed lines) for both the signal and idler photons (the signal and idler are defined as the higher and lower frequency bands, respectively). The pulse shaper is also used to compensate for undesired dispersion from the nonlinear crystals as well as connecting fiber links, and will subsequently be used to apply amplitude and spectral phase filters for the near-field mapping demonstrations. Upon leaving the pulse shaper, the biphotons are sent into the second PPLN waveguide (whose phase-matching peak is aligned with the first through temperature control), where the signal and idler photons are recombined via sum-frequency generation (SFG), also with a conversion efficiency of 10^{-5} [21]. The SFG photons at

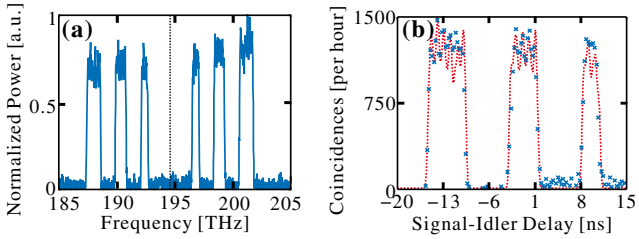

Fig. 1. Depiction of far-field frequency-to-time mapping. (a) The biphoton spectrum measured after three rectangular filters are applied on both the signal and idler sides. (b) The temporal correlation of the biphotons after propagating through a chirped fiber Bragg grating with $A_2 = 5200$ ps^2. The blue markers are the measured data points (acquired using a pair of single-photon detectors and an event timer), while the red dashed trace is the theoretical prediction.

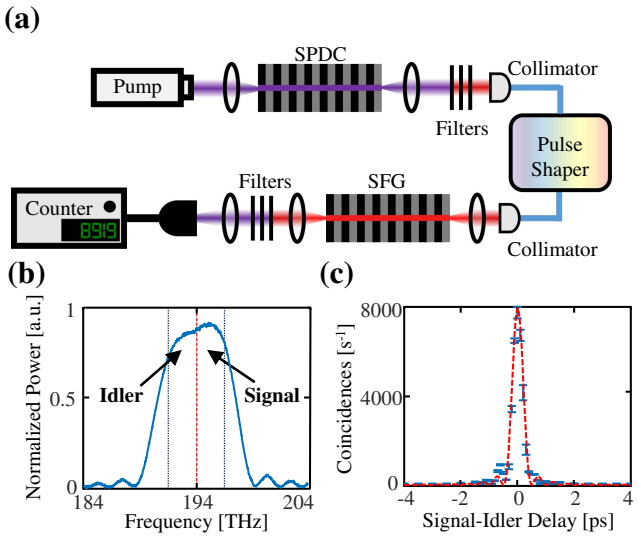

Fig. 2. (a) Experimental setup. (b) The biphoton spectrum measured directly after the first collimator. The dashed lines represent the 2.5 THz signal and idler passbands of the pulse shaper. (c) The measured temporal correlation function when the setup dispersion is compensated by the pulse shaper. The error bars give the standard deviation of five 1 s measurements, and the dashed curve represents the theoretical result. SPDC, spontaneous parametric downconversion; SFG, sum-frequency generation.

774 nm are detected on a silicon single-photon avalanche photodiode (PicoQuant τ-SPAD) with a dark count rate less than 20 s^{-1}, while the unconverted biphotons are filtered out. To sweep the delay necessary for the temporal correlation measurement, we use the pulse shaper to apply an additional linear spectral phase onto the signal spectrum, the slope of which corresponds to a relative delay between the signal and idler. Recording the upconverted photon counts then provides us a direct measurement of $G^{(2)}(\tau)$ with subpicosecond resolution [5,21]. As shown in Fig. 2(c), a single-peak correlation function with a full width at half-maximum (FWHM) of ~400 fs is recorded at the optimized dispersion compensation. Each data point in the correlation plot is the average of five measurements after dark-count subtraction, with the error bars showing the standard deviation and dashed lines representing the expected results based on theory. The correlation width in Fig. 2(c) is also an indicator of the finest temporal feature achievable with our setup, since the pulse shaper is incapable of increasing the optical bandwidth. Detailed analysis, albeit in the context of RF arbitrary waveform generation, can be found in [16].

To perform FTM, we start with programming the desired spectral shapes on the biphoton spectrum via the pulse shaper. Since frequency entanglement ensures that the net transfer function on the biphoton is the product of the complex filters applied to the signal and idler photons, we choose to shape only signal photons and always leave the idlers untouched in these experiments. For our first demonstration, we implement a series of Gaussian filters with a linewidth of 210 GHz (FWHM) and a spacing of 600 GHz. Figure 3(a) shows the measured biphoton spectrum after applying the filters to the signal half. The temporal correlation is subsequently stretched by a quadratic spectral phase (with $A_2 = 0.6$ ps^2) programmed on the shaper, which emulates a 30-m-long Corning SMF-28e fiber. The output stretched temporal correlation, shown in Fig. 3(b), is seriously distorted as the far-field limit is strongly violated; as discussed in [16], the far-field condition is satisfied only when $A_2 \gg 1/\pi\delta f^2$, where δf is the finest spectral feature. In our case, since the smallest biphoton spectral feature is 210 GHz, the far-field condition is satisfied only for a dispersion constant larger than 7.2 ps^2. However, we can circumvent the far-field condition by utilizing the near-field approach. We use the pulse shaper to apply the frequency-domain equivalent of $\psi_{nf}(\tau')$ to the biphotons. Figure 3(c) shows the new biphoton spectrum; the amplitude and phase shapes are based on the absolute value squared and the phase of $\phi_{nf}(\Omega)$, respectively. The output temporal correlation in Fig. 3(d) now shows clearly mapped Gaussian peaks after being stretched again by the quadratic spectral phase.

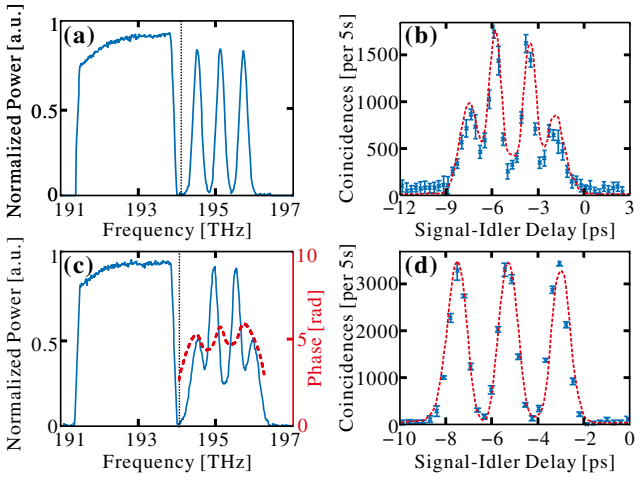

Fig. 3. (a) Biphoton spectrum measured after three Gaussian passbands, with a FWHM of 210 GHz and spaced by 600 GHz, are applied via the pulse shaper. (b) The temporal correlation measured after a quadratic spectral phase with an A_2 value of 0.6 ps^2 is applied on the spectrum in (a). (c) The preadjusted biphoton spectrum (solid; obtained by OSA) and extra spectral phases (dashed; programmed on the pulse shaper) needed to facilitate near-field FTM. (d) The measured temporal correlation utilizing the near-field FTM method is in good accordance with theoretical prediction.

Next, to show the flexibility of the near-field FTM method, we implement a pair of triangular shapes (FWHM of each triangle is 300 GHz) on the biphoton spectrum and the corresponding results are shown in Figs. 4(a)–4(d). Here, again, the far-field condition is violated, which results in a measured temporal correlation that is distorted after being stretched by the same amount of the quadratic spectral phase ($A_2 = 0.6$ ps^2, while 3.5 ps^2 is the minimum needed for far-field mapping). However, clear mapping can be achieved once the specific complex filter is computed in advance and applied to the biphotons before the dispersive propagation. A closer look at the results also reveals that the orientation of the triangles in the correlation plot [Fig. 4(d)] is flipped when compared to the applied masks [Fig. 4(a)]. This is due to the sign of A_2; the oppositely signed dispersion constant will ensure that the orientation of the triangles in the temporal measurement is the same as that of the initial spectral masks.

At this point, it is also worth noting that the optical power spectrum shaped for near-field FTM mirrors the distorted temporal correlation, as can be observed in Figs. 3(b), 3(c), and 4(b), 4(c). The spectral mask applied to the biphotons for near-field FTM is the frequency-domain counterpart of $\psi_{nf}(\tau')$ in Eq. (5), which can be written as

$$\phi_{nf}(\Omega) = \int d\tau' \psi_{in}(\tau') e^{i\tau'^2/2A_2} e^{i\Omega\tau'}. \quad (6)$$

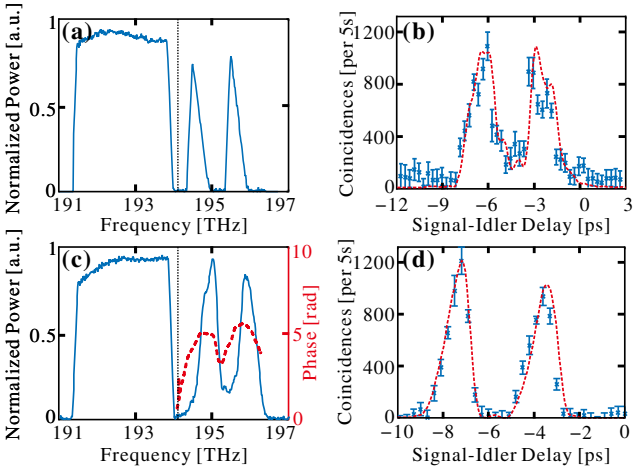

Fig. 4. (a) Biphoton spectrum and (b) the temporal correlation measured after amplitude filtering and a quadratic phase with an A_2 value of 0.6 ps^2 applied. (c) The preadjusted biphoton spectrum and (d) the measured temporal correlation utilizing the near-field FTM method.

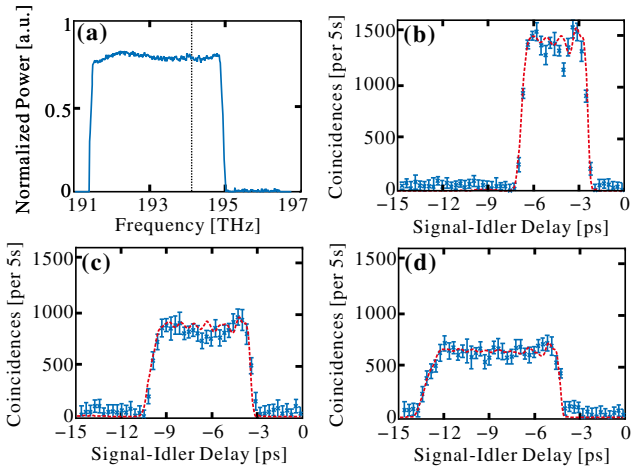

Fig. 5. (a) Biphoton spectrum measured after a rectangular filter, with a FWHM of 1 THz, is applied on the signal side. The measured temporal correlations after a quadratic phase with A_2 values of (b) 0.8, (c) 1.2, and (d) 1.6 ps^2 applied after the near-field FTM correction show good agreement with the theoretical curves. The measured FWHM values are 4.4, 6.7, and 8.9 ps, respectively.

Thus, we can observe a one-to-one correspondence when we compare the form of $\phi_{\mathrm{nf}}(\Omega)$ to that of $\psi(\tau)$ in Eq. (2), which explains the similarity between the distorted temporal correlation and the near-field corrected optical power spectrum.

We also emphasize that the near-field mask is complex, composed of not only an amplitude but also a phase that varies depending on the specifications of the target temporal correlation. As can be seen, the applied spectral phase in Fig. 4(c) is distinct from that applied in Fig. 3(c). Even though the phases here are only a few radians, they are vital for successful implementation of this technique, whereas in the far-field limit, the correlation is insensitive to the spectral phase of the input.

Finally, for a target shape, the near-field FTM method possesses a strong tunability in controlling the temporal correlation width, while maintaining the total photon flux. Although the preadjusted complex biphoton spectrum $\phi_{\mathrm{nf}}(\Omega)$ is dependent on the amount of dispersion available [Eq. (6)], the spectral energy remains constant. This can be understood through Parseval's theorem,

$$\frac{1}{2\pi}\int \mathrm{d}\Omega |\phi_{\mathrm{nf}}(\Omega)|^2 = \int \mathrm{d}\tau' |\psi_{\mathrm{nf}}(\tau')|^2, \tag{7}$$

which allows us to compute the spectral energy of the biphoton in the temporal domain. Since using Eq. (5) $|\psi_{\mathrm{nf}}(\tau')|^2 = |\psi_{\mathrm{in}}(\tau')|^2$, we can infer that the spectral energy of the near-field corrected biphoton is always equal to the energy of the input wave packet and does not depend on dispersion. Experimentally, we illustrate this property of strong tunability by using different dispersion values to obtain a rectangular target shape. Figure 5(a) provides the biphoton spectrum after applying a rectangular filter with a FWHM of 1 THz. We then compute and preadjust the biphoton spectrum to explore the near-field FTM for three different dispersion parameters, $A_2 = 0.8$, 1.2, and 1.6 ps^2, insufficient to meet the far-field condition. The corresponding measured temporal correlations shown in Figs. 5(b)–5(d) demonstrate excellent mapping to the target waveform, with a FWHM of 4.4, 6.7, and 8.9 ps, respectively, in close agreement with theoretical predictions. Moreover, the maximum coincidence counts recorded in Figs. 5(b)–5(d) are ~1400, ~930, and ~700 per 5 s, respectively, from which we obtain a correlation width-height product of 6160, 6231, and 6230 counts per 5 s, respectively. This suggests that the total photon-pair flux stays almost constant, even in the presence of different A_2 values.

In summary, we have shown that the proposed near-field FTM scheme can create arbitrary temporal correlation functions in the picosecond region. By preadjusting the complex biphoton spectrum with a Fourier-transform pulse shaper, the target shape can be mapped onto the biphoton temporal waveform after propagating through a small amount of dispersion. Unlike amplitude-only filtering, which results in a reduction of the biphoton flux to achieve longer temporal correlations, this near-field mapping approach synthesizes both amplitude and phase filtering for the efficient shaping of biphotons.

Funding. National Science Foundation (NSF) (ECCS-1407620).

Acknowledgment. We thank C. Langrock and M. M. Fejer for fabrication of the PPLN waveguides and acknowledge discussions with J. M. Lukens and P. Imany.

†These authors contributed equally to this work.

REFERENCES

1. J. L. O'Brien, A. Furusawa, and J. Vučković, Nat. Photonics **3**, 687 (2009).
2. A. Valencia, M. V. Chekhova, A. Trifonov, and Y. Shih, Phys. Rev. Lett. **88**, 183601 (2002).
3. S.-Y. Baek, O. Kwon, and Y.-H. Kim, Phys. Rev. A **77**, 013829 (2008).
4. A. O. Davis, P. M. Saulnier, M. Karpiński, and B. J. Smith, Opt. Express **25**, 12804 (2017).
5. A. Pe'er, B. Dayan, A. A. Friesem, and Y. Silberberg, Phys. Rev. Lett. **94**, 073601 (2005).
6. J. M. Lukens, A. Dezfooliyan, C. Langrock, M. M. Fejer, D. E. Leaird, and A. M. Weiner, Phys. Rev. Lett. **112**, 133602 (2014).
7. P. Kolchin, C. Belthangady, S. Du, G. Y. Yin, and S. E. Harris, Phys. Rev. Lett. **101**, 103601 (2008).
8. J. M. Lukens, O. D. Odele, D. E. Leaird, and A. M. Weiner, Opt. Lett. **40**, 5331 (2015).
9. S. Mittal, V. V. Orre, A. Restelli, R. Salem, E. A. Goldschmidt, and M. Hafezi, Phys. Rev. A **96**, 043807 (2017).
10. D. Kielpinski, J. F. Corney, and H. M. Wiseman, Phys. Rev. Lett. **106**, 130501 (2011).
11. J. M. Donohue, M. Agnew, J. Lavoie, and K. J. Resch, Phys. Rev. Lett. **111**, 153602 (2013).
12. C. Lee, Z. Zhang, G. R. Steinbrecher, H. Zhou, J. Mower, T. Zhong, L. Wang, X. Hu, R. D. Horansky, V. B. Verma, A. E. Lita, R. P. Mirin, F. Marsili, M. D. Shaw, N. S. Woo, G. W. Wornell, F. N. C. Wong, J. H. Shapiro, and D. Englund, Phys. Rev. A **90**, 062331 (2014).
13. C. Liu, Y. Sun, L. Zhao, S. Zhang, M. M. T. Loy, and S. Du, Phys. Rev. Lett. **113**, 133601 (2014).
14. J. M. Lukens and P. Lougovski, Optica **4**, 8 (2017).
15. J. A. Jaramillo-Villegas, P. Imany, O. D. Odele, D. E. Leaird, Z.-Y. Ou, M. Qi, and A. M. Weiner, Optica **4**, 655 (2017).
16. A. Dezfooliyan and A. M. Weiner, Opt. Express **21**, 22974 (2013).
17. Y. Shih, Rep. Prog. Phys. **66**, 1009 (2003).
18. B. H. Kolner and M. Nazarathy, Opt. Lett. **14**, 630 (1989).
19. M. Karpinski, M. Jachura, L. J. Wright, and B. J. Smith, Nat. Photonics **11**, 53 (2017).
20. A. M. Weiner, Rev. Sci. Instrum. **71**, 1929 (2000).
21. J. M. Lukens, A. Dezfooliyan, C. Langrock, M. M. Fejer, D. E. Leaird, and A. M. Weiner, Phys. Rev. Lett. **111**, 193603 (2013).